IPNO 00 – 01

Fast neutron distributions from Be and C thick targets bombarded with 80 and 160 MeV deuterons

N. Pauwels, S. Brandenburg, H. Laurent,
J. P. M. Beijers, F. Clapier, L. Lebreton
M. Mirea, M. G. Saint-Laurent, R. G. T. Zegers

EPJ manuscript No.
(will be inserted by the editor)

Fast neutron distributions from Be and C thick targets bombarded with 80 and 160 MeV deuterons

N. Pauwels[1], S. Brandenburg[2], H. Laurent[1], J.P.M. Beijers[2], F. Clapier[1], L. Lebreton[3], M. Mirea[4], M.G. Saint–Laurent[5], and R.G.T. Zegers[2]

[1] Institut de Physique Nucléaire, 91406, Orsay Cedex, France

[2] Kernfysisch Versnsneller Instituut, 9747 AA, Groningen, The Netherlands

[3] Université Catholique de Louvain, B–1348, Louvain–la–Neuve, Belgium

[4] Institute of Nuclear Physics and Engineering, P.O.Box MG–6, Bucarest, Romania

[5] Grand Accélérateur National d'Ions Lourds, BP 5027, 14021, Caen Cedex, France

the date of receipt and acceptance should be inserted later

Abstract. Measured angular and energy distributions of neutrons obtained by bombarding Be and C thick targets with deuterons at 80 and 160 MeV incident energies are reported. The data were obtained using the time–of–flight method. The experimental values are compared with a modelization based on stripping formalism extended for thick targets.

PACS. 28.20.-v Neutron physics – 29.25.Dz Neutron sources

1 Introduction

Production of fast neutrons studies have come to the fore in the past few years because of the great interest for the possible applications of induced fission to produce neutron rich ion beams. In this context, the main objective of the SPIRAL II (Système de Production d'Ions Radioactifs Accélérés en Ligne) and PARRNe (Production d'Atomes Radioactifs Riches en Neutrons) [1,2] R&D projects is the investigation of the feasibility and of the optimum parameters for a neutron rich isotope source. Special attention is dedicated to the energy and angular distributions of the neutrons obtained through deuteron break–up in different types of converters and different incident energies. Analysis and modelization of such behaviors, together with the study of the yields of neutron induced fission [3,4], can be used to optimize the productivity of the fissioning target it's geometry and designing it accordingly. The present

paper continues our previous studies realised for 17, 20, 28 [5] and 200 MeV [6] deuteron energies and it is focused on deuteron incident energies of 80 and 160 MeV.

2 Experimental procedure

In the experiment, the double differential cross section for neutron production induced by 80 and 160 MeV deuterons impinging on thick C and Be targets, in which the incident deuterons were complete stopped, have been measured.

The neutrons were detected with an array consisting of the 40 detectors from the EDEN [7] system (diameter 20 cm; thickness 5 cm; NE213 liquid scintillator) and 6 detectors from the DEMON–setup [8] (diameter 16 cm; thickness 20 cm; BC503 liquid scintillator). Neutron–gamma separation through pulse shape discrimination was performed by integrating the pulse with two different integration periods.

The detection thresholds for the neutron detectors were determined using sources of ^{137}Cs, ^{22}Na and ^{241}Am. They were set at 150 keV electron equivalent. The neutron detection efficiencies were calculated using the codes KENSTATE. Comparison of the calculations to data available for both type of detectors as well as comparison between the results from the different codes show a good agreement [9].

The energy of the neutrons was determined from the time–of–flight (TOF) measurement. To obtain an energy resolution of about 4% for the fastest, forward–emitted neutrons, which have approximately beam velocity, the length of the flightpath for the detectors at angles up to 30° was chosen to be 6 m. At backward angles, where the neutron energies are lower, a shorter flightpath was chosen. A schematic drawing of the setup is shown in Fig. 1.

As the TOF of the neutrons is considerably larger than the period between the buckets from the cyclotron it is not possible to know unambiguously from which bucket the detected neutron originates and to derive the start for the TOF from the cyclotron RF–signal, when all buckets are filled. Since the AGOR–cyclotron is not equipped to control the contents of the buckets on a bucket–to–bucket basis, the only possible method to determine the start of the TOF is to detect the arrival of the individual deuterons at the target.

The incident deuterons were detected with a 2 mm thick NE102A scintillator slab mounted in front of the target, which was viewed by an XP2020 photomultiplier tube. The efficiency of the tagging detector was measured to be essentially 100% by comparing its singles countrate with the coincident countrate between the tagging detector and one of the neutron detector, mounted at the position of the target. No significant deterioration of the gain of the tagging detector was observed up to a countrate of 10^6 cps. It was furthermore observed that the countrate of the tagging detector was to better than 1% proportional with the current extracted from the ion source up to a countrate of 10^6 cps.

The timing between the tagging detector and the neutron detectors was arranged such that coincidences corresponding to prompt γ–rays were located in the middle of

the 1 μs coincidence window, thus allowing the first half of the window to be used for subtraction of random coincidences between deuterons arriving at the target and neutron detectors triggering on room background not correlated with the beam. A pile–up inspection window of 1 μs was used for the tagging detector to lift ambiguities due to a second deuteron arriving within the coincidence window. Using a beam intensity of 10^5 deuterons per second the dead–time due to pile–up amounted to 10%. It was measured by comparing the number of deuterons arriving at the target and the number of accepted deuteron triggers. At this intensity, the probability of finding two deuterons in one bucket or in adjacent buckets, which will not be detected by the pile–up inspection is about 1%.

The overall detection efficiency of the setup was $\mathcal{O}(10^{-3})$, thus leading to a neutron countrate $\mathcal{O}(10^2)$ and a similar background countrate. The deadtime of the electronics and the data–acquisition at this rate was of the order of a few percent. It was monitored by comparing the number of accepted deuteron triggers with the number of downscaled deuteron singles events accepted by the data–acquisition system. The beam intensity required for the experiment is well below the detection limit of the diagnostic tools in the cyclotron and beam line. The relative difference in the charge–to–mass ratio (Q/A) between molecular hydrogen ions and deuterons is 6.6×10^{-4}. This difference is large enough to ensure a complete separation of the two species by the cyclotron, but small enough to allow switching between the two beams by only adjusting the RF–frequency of the cyclotron. The low intensity of the deuteron beam was obtained by exploiting the 1.5×10^{-4} abundance of deuterium in natural hydrogen. To obtain a beam of 10^5 deuterons per second on target, a molecular hydrogen beam of about 20 nA was extracted from the ion source. This was achieved by closing the emittance defining slits at the exit of the ion source. Furthermore, the injection efficiency was deteriorated to about 1% by operating the buncher 180° out of phase with respect to the normal setting. Fine adjustment of the beam intensity was done by changing the buncher phase and amplitude.

A 100 mm thick Be target and a 70 mm thick C target were used. The targets presents a cylindrical form, 30 mm in diameters and were surrounded by an iron shield to prevent the escape of protons and other charged particles. These target dimensions are sufficient to stop the incident deuterons. The distances between the target and the detectors were measured considering the mass center of the target as the reference. The experiment was monitored by counting the deuteron detected in the plastic, downscaled by a factor 10^3. The overall efficiency for neutron detection was roughly 4×10^{-4}. The total neutron counting rate was about 40 s^{-1}. The experiment has been performed at 80 MeV and 160 MeV for both targets. The data recorded during the runs were unfolded using the OASIS-IPN package.

3 Results and discussion

In the following, angular and energy distributions of neutrons obtained by bombarding Be and C thick targets with incident deuterons of 80 and 160 MeV are reported,

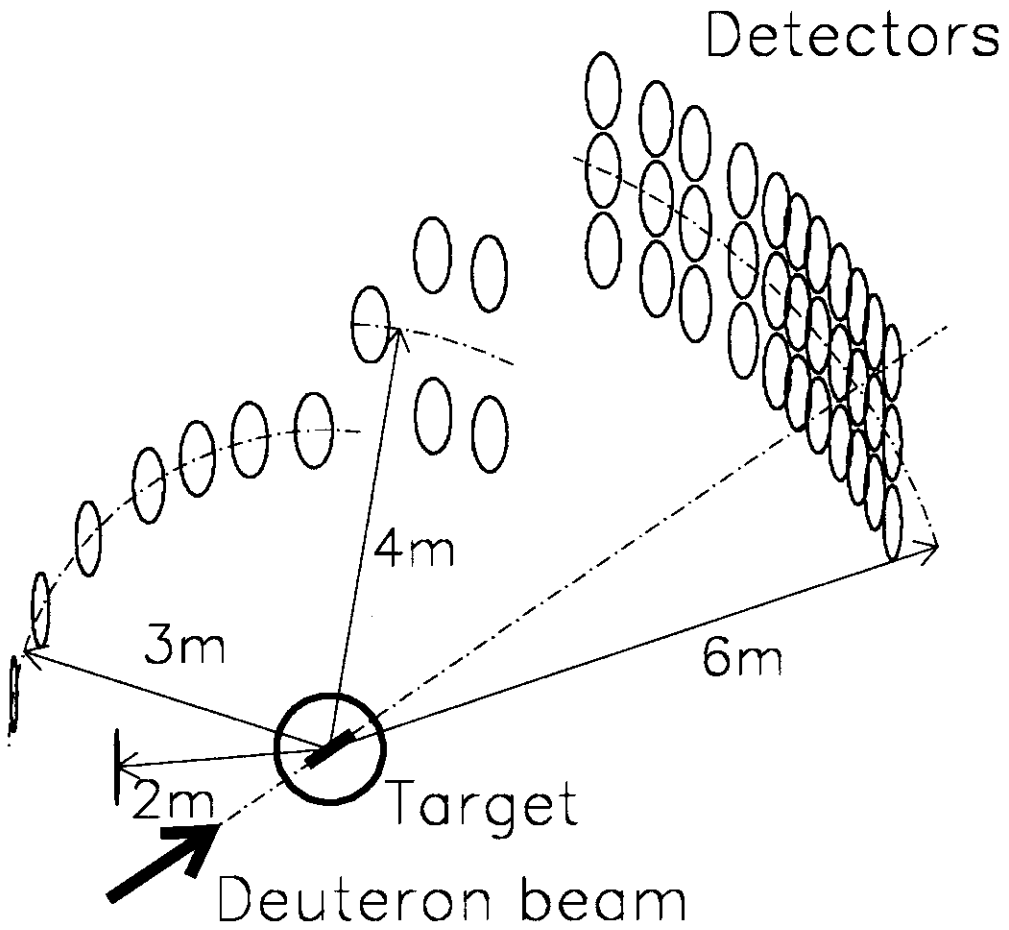

Fig. 1. Experimental set–up.

scanning a large energy interval where quantitative data were not available. However, some information about the characteristics of the neutron distributions at 160 MeV deuteron energy exist [10,11] from many years, but the authors reported only the relative values of the measurements. The detectors placed at the angles 2.3°, 3.3°, 6.2°, 8.4°, 11.1°, 15.1°, 20.3° and 33.3°, covering the forward direction region, were selected for examination. For the future activities, a simple phenomenological formalism intended to simulate the distributions in the forward direction represents a very useful tool. So, the experimental results are compared with phenomenologic simulations obtained by extending the formalism based on Serber's theory [12] presented in details in Ref.[5]. Following the Serber's prescriptions, two distributions can be modelized semi–classically in the case of thin targets: one distribution is due to the stripping reaction and another is due to direct collisions between nucleons, resulting in the escape of some particles from the target nucleus. For an initial deuteron energy, these distributions determine the neutron probability to be emitted at an angle θ at an energy E_n. In the case of thick targets, this probability must be integrated over the deuteron range weighted with the cross section (d, n). Theoretical angular and energy neutron yields followed by renormalizing the integrated probability with the experimental value of the total yield at

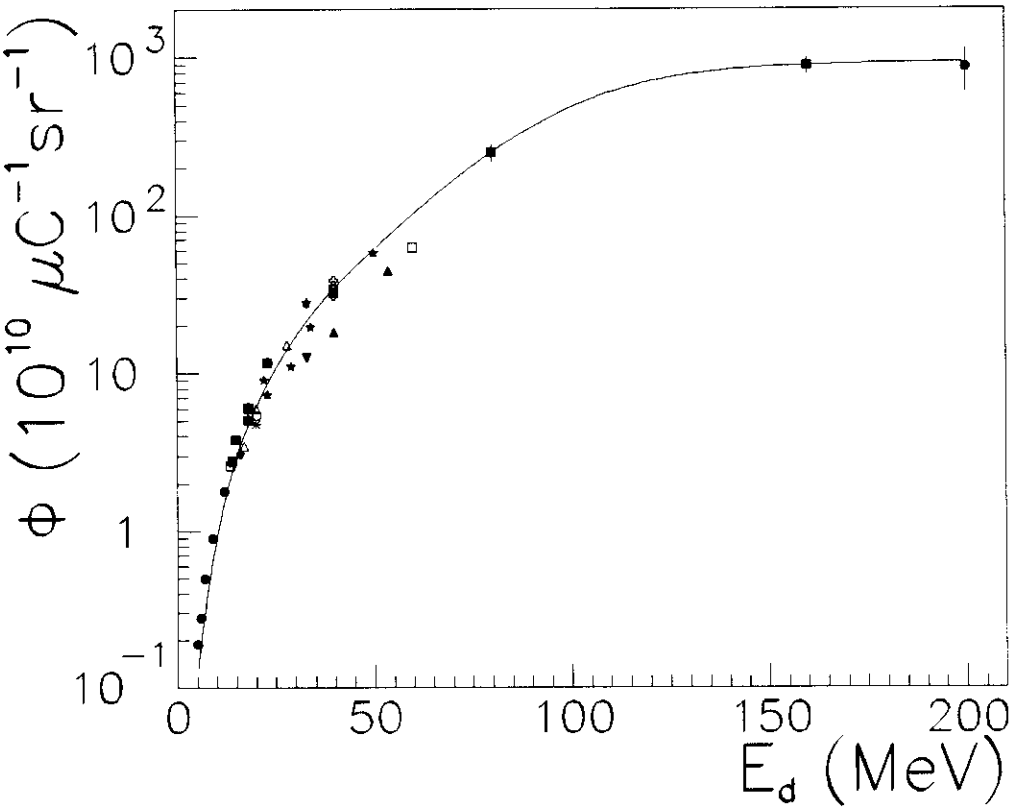

Fig. 2. A systematic of total yields Φ at 0° versus the incident energy of the deuteron E_d for the bombardment of Be is obtained by plotting experimental results given in different references: filled circles from Ref. [14] (5, 6, 7, 9, 12, 18 and 23 MeV), filled squares from Ref. [15] (14, 14.8, 18, 23 and 40 MeV), up–point filled triangles deduced from Ref. [16] (40 and 53.8 MeV), down–point filled triangle from Ref. [17] (12.5 MeV), empty circle from Ref. [18] (20.2 MeV), empty square from Ref. [13] (13.54 MeV), up–point empty triangles from [5] (17, 20 and 28 MeV), empty rhombs from Ref. [19] (16, 33 and 50 MeV), empty crosses from Ref. [20] (4 points at 40 MeV), filled stars from the compilation of Ref. [21] (14, 16, 18, 22, 23, 29, 33, 34, 40 and 50 MeV), empty stars from Ref. [22] (14.8, 18 and 23 MeV), asterisk from Ref. [23] (20 MeV), filled circle at E_d=200 MeV from Ref. [6], empty square at 60 MeV deduced from Ref. [24], filled squares at 80 and 160 MeV from the present study. In the low energy deuteron energy the plot looks like with the curve drawn in Ref. [25]. The curve is obtained with the semi–empirical parametrization given by Rel. (1).

0°. This formalism needs, first of all, an estimation of the neutron yields at 0° for thick Be targets as function of the deuterons incident energies. This dependence gives the approximate productivities for other kinds of targets by using simple geometric relations involving atomic and mass numbers of the concerned elements. Semi–empirical formulae for this quantity are given in the Ref. [13] (for incident energies smaller than 15 MeV) and Ref. [14] (over 15 MeV), but their validity becomes uncertain for deuteron energies greater than 50 MeV due to the lack of experimental data over this value. Using the experimental yields obtained in Ref. [6] and the present work, together with

a systematic of experimental data, a fit of the data has been made and the following formula is proposed for the yields at 0° up to 200 MeV deuteron incident energy on thick Be targets:

$$Y(\theta = 0°)/Q = \begin{cases} 10.1 \times 10^{12} E_d^{2.95} & \text{for } E_d < 15 \text{ MeV}, \\ 3.4 \times 10^{13} E_d^{2.5} & \text{for } 15 \text{ MeV} \leq E_d \leq 50 \text{ MeV}, \\ \left\{ \frac{928.3}{1+\exp[0.053(98-E_d)]} - 6.89 \right\} \times 10^{16} & \text{for } 50 \text{ MeV} < E_d, \end{cases} \quad (1)$$

where Y/Q is the number of neutrons over the incident charge unit in $sr^{-1}C^{-1}$ and the incident energy of the deuteron E_d is given in MeV. Fig. 2 displays the experimental data together with the semi–empirical curve. A word about the accuracy of experimental data: it was emphasized [14,22] that the neutron with energies below 2 MeV yield decreases from 33% of the total yield at E_d=10 MeV to about 15% at E_d=25 MeV. In general, the experimental values were measured with a neutron threshold of 2–4 MeV, and the relative cut–off error is similar for almost all the data displayed. In this context, the very low neutron productivities given by the up–point filled triangles located at E_d=40 and 53.8 MeV incident deuteron energies extracted from Ref. [16] are due essentially to the detection threshold in neutron energy of about 10 MeV. The data obtained using time of flight techniques proved to be consistent with those obtained from activation measurements [20] (E_d=40 MeV).

One choice for the dependence of the forward direction cross section in the Be target is given by the formula [15]

$$\left.\frac{d\sigma(E)}{d\Omega}\right|_{\theta = 0°} = 0.18\ln(E) + 0.007E \quad (2)$$

and another proposed dependence [5] as

$$\left.\frac{d\sigma(E)}{d\Omega}\right|_{\theta = 0°} = 2. \times 10^{-4} E^{1.5} \left|\frac{dE}{dt}\right| \quad (3)$$

where dE/dt is the stopping power in MeV/(g/cm^2), E is the deuteron energy in MeV for the range t in the target, and the cross section is expressed in b/sr. Both approximations were used in calculations up to 40–50 MeV deuteron energies. In the following, the dependences exhibited by these formulae were extrapolated for all the energy domain concerned with the imposed restriction that when σ reaches the value 1.35 b, this value being regarded as an upper limit [24], σ remains constant. In this context, it was considered that at the highest energies, the major part of the cross section is concentrated in the forward direction. The theoretical simulations for incident deuteron at energies of 80 and 160 MeV obtained by using these two parametrizations [Rels. (2) and (3)] were almost identical. Also, as usually done for thick targets, an attenuation of the initial beam was taken into account by multiplying the cross section with a factor directed by a law of the type $\exp(-\int N\sigma\ dt)$, where $\int N\ dt$ is the number of nuclei on the surface unit. Another modification of the formalism of Ref. [5] is that the straggling angle is computed by extrapolating the table of Ref. [26] as function of the deuteron position in the target while in our previous work [5] the mean value over the range of the deuteron was considered.

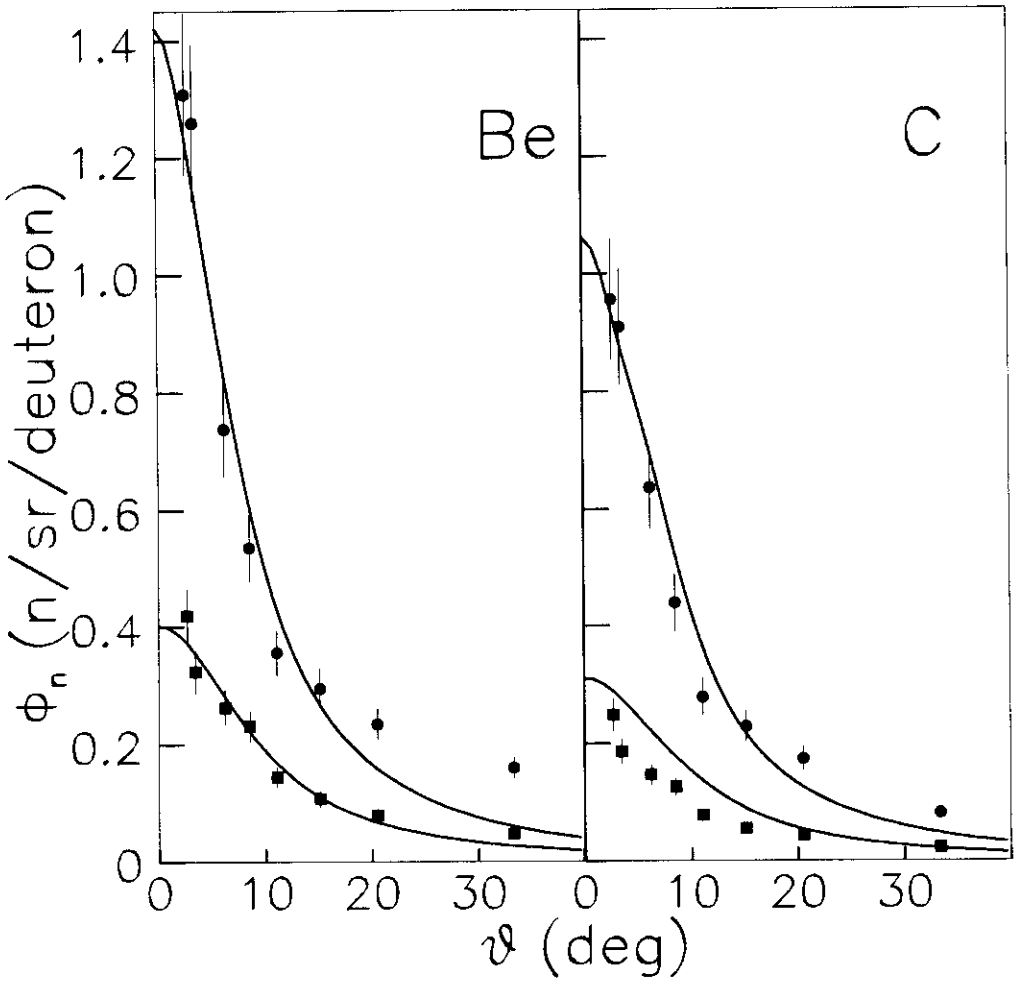

Fig. 3. Angular neutron distributions Φ_n versus the detection angle θ for Be and C targets (the nature of the target is marked on the plots). The filled squares correspond to the deuteron incident energy of E_d=80 MeV while the filled circles correspond to E_d=160 MeV. The integration neutron energy thresholds were set at 4 MeV. The full curves represent the simulations.

The neutron angular distributions Φ_n are represented in Fig. 3 versus the detection angle θ. At both incident deuteron energies (E_d=80 and 160 MeV), the neutron yields delivered by the Be thick target are greater than those obtained from the C one with a factor of about 1.3–1.4. Also, the angular distributions for the Be target are narrower than those for the C one at each deuteron incident energy, reflecting mainly that the scattering of the deuteron by the Coulomb field is stronger in the C target. As expected, for both targets at lower incident energy, the distributions are larger because, according to the Serber's theory, the mean scattering angle is inversely proportional to the deuteron kinetic energy. A comparison is presented in Fig. 3 with the calculated distributions. The experimental values are reasonably reproduced up to $\theta = 15°$, above large discrepancies appearing between the theory and the experiment. These differences are mainly due to the neutrons detected from the evaporation process which are not taken into account in the simulation. Concerning the PARRNe project, it is important to note that the ma-

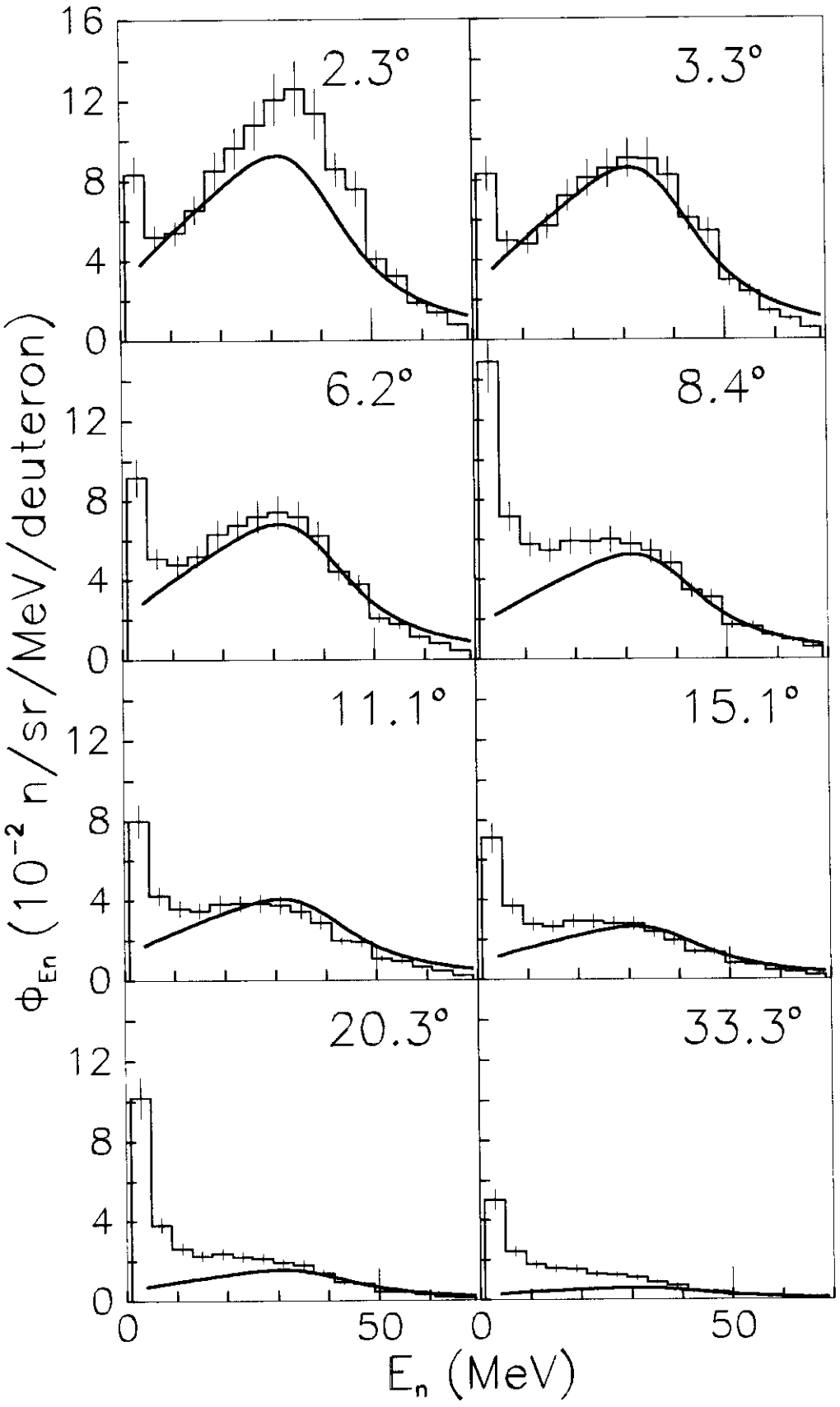

Fig. 4. Neutron energy distributions Φ_{En} at different detection angles versus the neutron energy E_n in the case of the Be target for an incident deuteron energy of E_d=80 MeV. The curves represent the simulations.

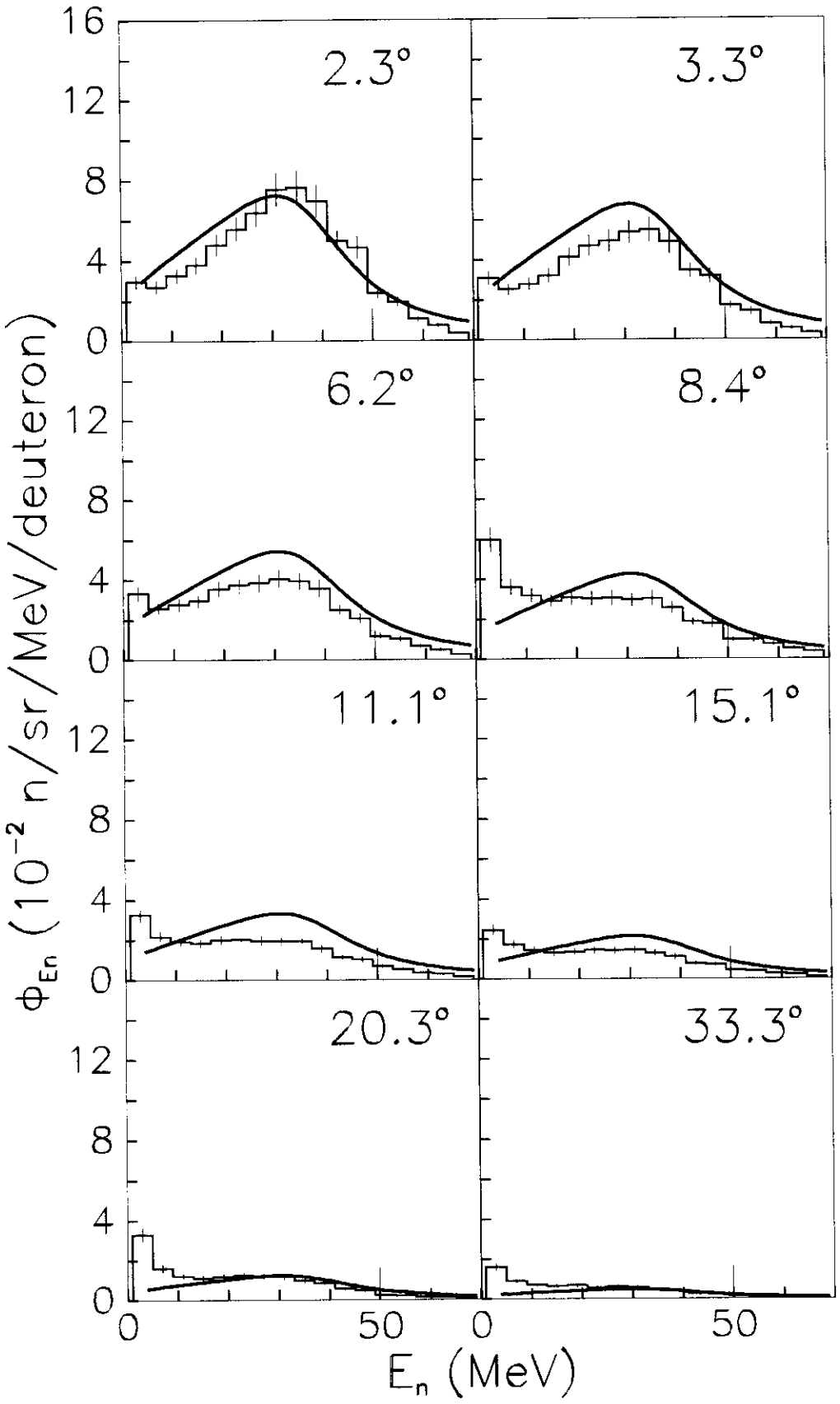

Fig. 5. Neutron energy distributions Φ_{En} at different detection angles versus the neutron energy E_n in the case of the C target for an incident deuteron energy of E_d=80 MeV. The curves represent the simulations.

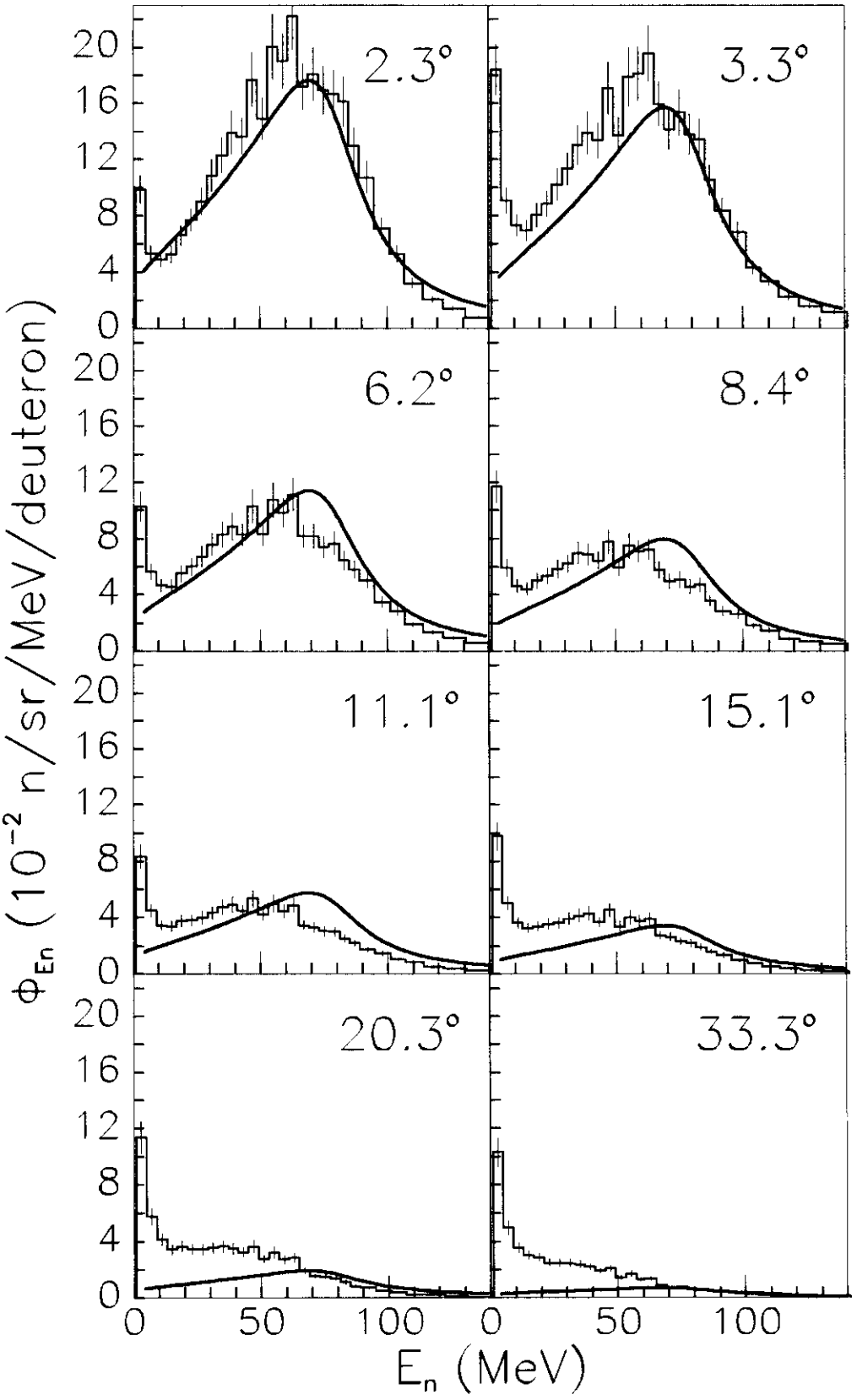

Fig. 6. Neutron energy distributions Φ_{En} at different detection angles versus the neutron energy E_n in the case of the Be target for an incident deuteron energy of E_d=160 MeV. The curves represent the simulations.

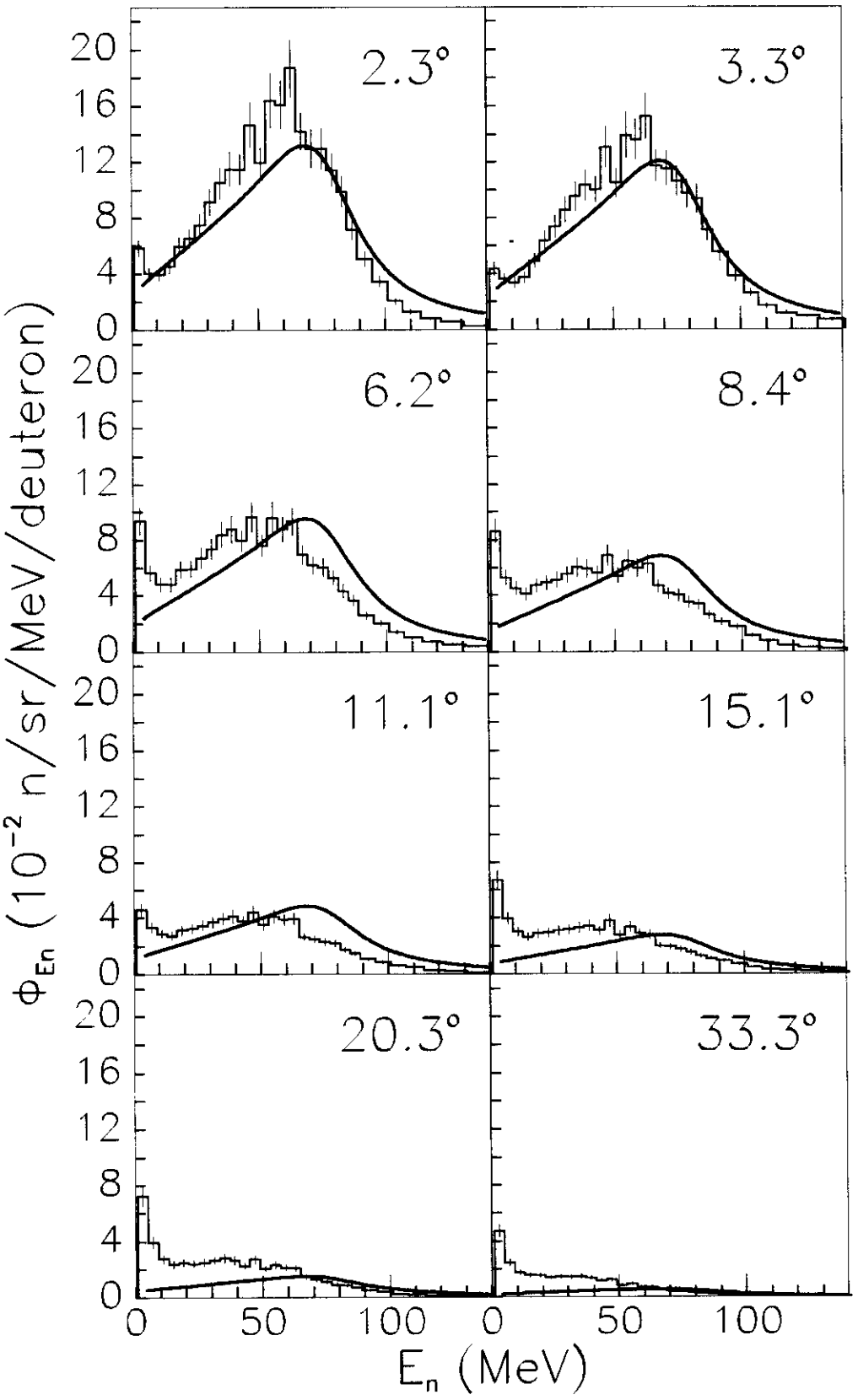

Fig. 7. Neutron energy distributions Φ_{En} at different detection angles versus the neutron energy E_n in the case of the C target for an incident deuteron energy of E_d=160 MeV. The curves represent the simulations.

jor part of the neutron yield is delivered in a small angular region around $\theta = 0°$, the full widths at half maximum being 7.1° and 8.3° at 160 MeV incident deuteron energy, 9.2° and 9.3° at 80 MeV, for Be and C targets, respectively. For both targets, the neutron yields delivered in the forward direction are about 3.5 times greater at the 160 MeV incident energy than those at 80 MeV.

The energy distributions Φ_{En} in the forward direction are shown in Figs. 4, 5, 6 and 7. In the case of the Be target and of the incident deuteron energy E_d=80 MeV, the energy distribution curves Φ_{En} are represented in Fig. 4. At the low angles ranging up to 15.1°, the energy dependences of the yields clearly exhibit two well known regions of interest: the low energy part of the flux (for neutron energies E_n up to 15 MeV) which corresponds mainly to neutrons due to the evaporation and the high energy part which is characterized by a peak located at a most probable neutron energy (lower than half of the incident deuteron energy), assumed to result from direct collisions between the projectile and the target nuclei. This peak is asymmetric, exhibiting a more pronounced slope on its right side. The neutron yield produced by evaporation is practically isotropic, so that the intensity of the evaporation is almost constant over the angles. Concerning the second distribution, mainly due to the deuteron break–up, the position of the peak on the energy scale depends on the detection angle. Comparing the plots at different angles in Fig. 4, it can be observed that the position of the peak decreases slowly with the detection angle. When the laboratory angle increases over a certain value, in the case of Be target and E_d=80 MeV this value being approximatively 20°, the neutron yield produced by the projectile break–up is overridden by that due to the evaporation, accordingly the peak of most probable neutron energy vanishes. At 2.3°, the peak position is about at 33–34 MeV. The simulations reproduce the energy distributions due to the deuteron break–up, but the variations of the peak position in terms of energy scale as a function of the detection angle are not reproduced. At E_d=80 MeV and the C target, the energy distribution curves are represented in Fig. 5. The observations evidenced within the Be target are still valid.

In the case of the incident deuteron energy E_d=160 MeV and the Be target, the energy distribution curves are shown in Fig. 6. The most probable neutron energy is at approximatively E_n=60 MeV. The trend exhibited by this peak is similar to that observed for E_d=80 MeV. At the same energy, the behaviors of the energy distributions concerning the C target displayed by Fig. 7, are quite similars, differences arising quantitatively in the values of the yields, the Be target being more productive. In Figs. 6 and 7, the energy distributions are overestimated for energies up to $E_n \approx$60 MeV at 2.3°, 3.3°, 6.2° and 8.4°. This arises because it was not possible to discriminate recorded events due to some protons during the treatment of experimental data in the case of these detectors.

The neutron yields determined up to 20° are pertinent to our R&D program and offer an additional experimental guidance for our future work. In this energy region, our semi–empirical parametrization gives results which de-

scribe in a satisfactory manner the characteristics of the peak due to stripping and the values of the fast neutron yields. This type of simulation will provide an useful tool for the optimization of the converter–^{238}U target geometry at different incident deuteron energies to obtain the best productions of neutron–rich elements.

Acknowledgements

This work was sponsored by the European Contract SPIRAL II No. ERB 4062 PL 975009 and by IN2P3 No. FMGE CT 980100.

References

1. F. Clapier, A.C. Mueller, C. Obert, O. Bajeat, M. Ducourtieux, A. Ferro, A. Horbowa, L. Kotfila, C. Lau, H. Lefort, S. Kandry–Rody, N. Pauwels, J.C. Poitier, J. Proust, J.C. Putaux, C.F. Liang, P. Paris, A.C.C. Vilari, R. Lichtenhäler, L. Maunoury, and J. Lettry, Phys. Rev. ST Accel. Beams **1** (1998) 013501.
2. S. Kandri–Rody, J. Obert, E. Cottereau, O. Bajeat, M. Ducourtieux, C. Lau, H. Lefort, J.C. Poitier, J.C. Putaux, F. Clapier, J. Lettry, A.C. Mueller, N. Pauwels, J. Proust, C.F. Liang, P. Paris, H.L. Ravn, B. Roussiere, J. Sauvage, J.A. Scarpaci, F. Le Blanc, G. Lalu, I. Lhenry, T. Von Egidy and R. Antoni, Nucl. Instr. Meth. B **160** (2000) 1.
3. M. Mirea, F. Clapier, N. Pauwels, and J. Proust, Nuovo Cimento **111A** (1998) 267.
4. I.C. Gomes and J.A. Nolen, in Proc. of the 2nd Int. Topical Meeting on Nuclear Applications of Accelerator Technology, Gatlinburg, TN, USA, September 20–23, 1998; J.A. Nolen, private communication 1998.
5. S. Menard, M. Mirea, F. Clapier, N. Pauwels, J. Proust, C. Donzaud, D. Guillemaud–Mueller, I. Lhenry, A.C. Mueller, J.A. Scarpaci and O. Sorlin, Phys. Rev. ST Accel. Beams **2** (1999) 033501.
6. N. Pauwels, F. Clapier, P. Gara, M. Mirea and J. Proust, Nucl. Instr. Meth. B **160** (2000) 315.
7. H. Laurent, H. Lefort, D. Beaumel, Y. Blumenfeld, S. Fortier, S. Gales, J. Guillot, J.C. Roynette, P. Volkov and S. Brandenburg, Nucl. Instr. Meth. A **326** (1993) 517.
8. I. Tilquin, Y. El Masri, M. Parlog, Ph. Collon, M. Hadri, Th. Keutgen, J. Lehmann, P. Deleux, P. Lipnik, A. Ninane, F. Hanappe, G. Bizard, D. Durand, P. Mosrin, J. Peter, R. Regimbart and B. Tamain, Nucl. Instr. Meth. A **365** (1995) 446.
9. R.A. Cecil, B.D. Andersen and R. Madey, Nucl. Instr. Meth. **161** (1979) 439.
10. A.C. Helmholtz, E.M. McMillan and D.C. Sewell, Phys. Rev. **72** (1947) 1003.
11. W.J. Knox, Phys. Rev. **81** (1951) 687.
12. R. Serber, Phys. Rev. **72** (1947) 1008.
13. H.J. Brede, G. Dietze, K. Kudo, U.J. Schrewe, F. Tancu and C. Wen, Nucl. Instr. Meth. A **274** (1989) 332.
14. M.A. Lone, A.J. Ferguson and B.C. Robertson, Nucl. Instr. Meth. **189** (1981) 515.
15. D. Christenson, M.W. McNaughton and J.A. Jungerman, Nucl. Instr. Meth. **160** (1979) 499.
16. G.W. Schweimer, Nucl. Phys. A **100** (1967) 537.
17. Kazuo Shin, Kouki Hibi, Masahito Fujii, Yoshitomo Uwamino and Takashi Nakamura, Phys. Rev. C **29** (1984) 1307.
18. A. Belymam, A. Hoummada, J. Collot, P. de Saintignon, G. Mahout and B. Merkel, Nucl. Instr. Meth. B **134** (1998)

217.

19. J.P. Meulders, P. Leleux, P.C. Macq and C. Pirart, Phys. Med. Biol. **20** (1975) 235.
20. M.J. Saltmarsh, C.A. Ludemann, C.B. Fulmer and R.C. Styles, Nucl. Instr. Meth. **145** (1977) 81.
21. P. Grand and A.N. Goland, Nucl. Instr. Meth. **145** (1977) 49.
22. M.A. Lone, C.B. Bigham, J.S. Fraser, H.R. Schneider, T.K. Alexander, A.J. Ferguson and A.B. McDonald, Nucl. Instr. Meth. **143** (1977) 331.
23. J. Collot, P.De Saintignon, P. Gabor, A. Hoummada, G. Mahout, D. Marchand, F. Merchez, E. Leon Florian, C. Leroy, Ph. Jean and B. Merkel, Nucl. Instr. Meth. A **350** (1994) 532.
24. K. Goebel and A.J. Miller, Nucl. Instr. Meth. **96** (1971) 581.
25. J.A. Stokes, L.A. Parks, C.A. Preskitt and J. John, IEEE Trans. Nucl. Sci. **NS–30** (1983) 1623.
26. H. Bichsel, Preprint USC–136–150 (1970).